In mice and humans, brain microvascular contractility matures postnatally Brain microvessel post-natal maturation

Leila Slaoui
CNRS Unité Mixte de Recherche 724, INSERM Unité
Alice Gilbert
CNRS Unité Mixte de Recherche 724, INSERM Unité
Armelle Rancillac
CNRS Unité Mixte de Recherche 724, INSERM Unité
Audrey Chagnot
Normandie University, UNICAEN, Inserm, GIP Cyceron, Institut Blood and Brain @Caen-Normandie (BB@C), UMR-S U1237
Laetitia Federici
Université de Paris, UMRS-1144
Quentin Gerard
Normandie University, UNICAEN, Inserm, GIP Cyceron, Institut Blood and Brain @Caen-Normandie (BB@C), UMR-S U1237
Antoinette Gelot
Assistance Publique – Hôpitaux de Paris, AP-HP, Hôpital Universitaire – Necker – Enfants Malades
Mathilde Becmeur-Lefebvre
Assistance Publique – Hôpitaux de Paris, AP-HP, Hôpital Universitaire – Necker – Enfants Malades
Maryline Favier
Institut Cochin
Noémie Robil
Paris Biotech Santé
Gaëlle Letort
CNRS Unité Mixte de Recherche 724, INSERM Unité
Karine Dias
Institut de Biologie de l'ENS (IBENS), École normale supérieure, CNRS, INSERM, Université PSL
Laurent Jourdren
Institut de Biologie de l'ENS (IBENS), École normale supérieure, CNRS, INSERM, Université PSL
Philippe Mailly
CNRS Unité Mixte de Recherche 724, INSERM Unité
Sylvain Auvity

Université de Paris, UMRS-1144

Salvatore Cisternino

Université de Paris, UMRS-1144

Denis Vivien

Normandie University, UNICAEN, Inserm, GIP Cyceron, Institut Blood and Brain @Caen-Normandie (BB@C), UMR-S U1237

Martine Cohen-Salmon (martine.cohen-salmon@college-de-france.fr)

CNRS Unité Mixte de Recherche 724, INSERM Unité

Anne-Cécile Boulay

CNRS Unité Mixte de Recherche 724, INSERM Unité

Research Article

Keywords: Brain microvessels, Postnatal development, Vascular smooth muscle cell, microvessel contractility, Cerebral blood flow

Posted Date: May 11th, 2022

DOI: https://doi.org/10.21203/rs.3.rs-1608620/v1

Abstract

Although great efforts to characterize the embryonic phase of brain microvascular system development have been made, its postnatal maturation has barely been described. Here, we compared the molecular and functional properties of brain vascular cells on postnatal day (P)5 vs. P15, via a transcriptomic analysis of purified mouse cortical microvessels (MVs) and the identification of vascular-cell-type-specific or -preferentially expressed transcripts. We found that endothelial cells (EC), vascular smooth muscle cells (VSMC) and fibroblasts (FB) follow specific molecular maturation programs over this time period. Focusing on VSMCs, we showed that arteriolar VSMC network expands and becomes contractile resulting in a greater cerebral blood flow (CBF). Samples of human brain cortex showed the same postnatal maturation process. Thus, the postnatal phase is a critical period during which arteriolar VSMC contractility required for vessel tone and brain perfusion is acquired and mature.

Introduction

The brain's extremely dense microvascular system sustains the neurons' high metabolic demand by providing the cells with a regulated flow of blood and physically and functionally sheltering them from harmful components in the blood. These microvessels form a complex, heterogeneous network. Penetrating arterioles ramify into a dense capillary tree that converges into venules and then veins. These microvessels are composed of endothelial cells (ECs), which form the BBB that separates the blood from the parenchyma in most areas of the brain. ECs are contacted by various types of cell (Vanlandewijck et al. 2018). In the arteriolar network, ECs are surrounded by concentric, contractile VSMCs, which regulate vascular tone and blood perfusion (Rungta et al. 2018). The VSMCs become progressively sparser as the vessels branch and are present as discrete, non-contractile cells in veins (Frosen and Joutel 2018). Pericytes (PCs, another type of periendothelial mural cell) line the vessel walls of pre-capillary arterioles, capillaries, and post-capillary venules. Like VSMCs, PCs form a continuum that ranges from contractile cells around pre-capillary arterioles and capillaries to a mesh of star-shaped, non-contractile cells on post-capillary venules (Hartmann et al. 2015). Perivascular FBs are present around vessels other than capillaries (Saunders et al. 2018; Vanlandewijck et al. 2018). The FBs are highly heterogeneous and are thought to have various functions in extracellular matrix (ECM) composition, blood vessel contractility, and immune control (Saunders et al. 2018; Manberg et al. 2021). Lastly, perivascular astrocytic processes (also referred to as "endfeet") form a continuous sheath around all the vessels (Mathiisen et al. 2010) and control several vascular properties (i.e. BBB integrity, cerebral blood flow, perivascular homeostasis and immunity) (Cohen-Salmon et al. 2021).

In rodents, the brain's blood vessels start to develop on or around embryonic day (E) 9. Firstly, ECs from a vascular plexus formed by mesodermal angioblasts, invade the neuroectoderm and form intraneural vessels (Coelho-Santos et al. 2021; Coelho-Santos and Shih 2020). They start expressing junctional proteins as early as they enter the brain parenchyma (Ben-Zvi and Liebner 2021). This angiogenic phase is followed by a differentiation phase around E15, during which PCs and VSMCs are recruited to the endothelial surface, induce EC's BBB properties (such as the the inhibition of transcytosis), and thus

reduce paracellular molecular transfer and increase transcellular transport (Hellstrom et al. 1999; Daneman et al. 2010). Interestingly, a second wave of angiogenesis, vascular remodeling and BBB maturation occurs postnatally (Coelho-Santos et al. 2021; Coelho-Santos and Shih 2020) - suggesting that angiogenesis and BBB genesis are interlinked.

Although great efforts to characterize the embryonic phase of brain vascular development have been made, the exact time course, molecular bases and functional consequences of the system's postnatal maturation remain mainly unknown. By combining transcriptomic, biochemical, histochemical and functional assessments, we characterized the brain's microvascular compartment during postnatal development in mice and humans. Our results revealed that vascular cells follow a specific maturation program with important functional consequences on cerebral perfusion.

Material And Methods

Animal experiments and ethical approval

Mice were purchased from Janvier Labs (Le Genest-Saint-Isle, France) and kept in pathogen-free conditions. All animal experiments were carried out in compliance with (i) the European Directive 2010/63/EU on the protection of animals used for scientific purposes and (ii) the guidelines issued by the French National Animal Care and Use Committee (reference: 2013/118). The study was also approved by the French Ministry for Research and Higher Education's institutional review board. No gender distinction was made. All studies were performed on swiss mice except ex vivo VSMC contractility tests that were done on C57BL6 mice.

Microvessel (MV) purification

MVs were purified from dorsal cortex (for RNASeq analyses) or whole brain (for other experiments), as described previously (Boulay et al. 2015). A 100 µm-mesh negative filter and a 20 µm-mesh positive filter were used to enriched our preparation with arterioles, veinules and capillaries, and remove meninges large arteries and veins and cell debris.

RNA sequencing and analysis

Total mRNA was extracted from purified cortical MVs on P5 or P15, using the RNeasy Lipid Tissue Kit (Qiagen, Hilden, Germany). Ten ng of total RNA were amplified and converted into cDNA using a SMART-Seq v4 Ultra Low Input RNA Kit (Clontech). Next, an average of 150 pg of amplified cDNA per library were processed with a Nextera XT DNA Kit (Illumina). Libraries were multiplexed on two high-output flow cells and sequenced (using 75 bp reads) on a NextSeq 500 device (Illumina). The mean ± standard deviation (SD) number of reads meeting the Illumina quality criterion was 48 ± 5 million per sample. The RNA-seq gene expression data and raw fastq files are available on the GEO repository (www.ncbi.nlm.nih.gov/geo/) under the accession number GSE173844.

The RNA-Seq data were analyzed using GenoSplice technology (www.genosplice.com). Sequencing, data quality checks, read distribution checks (e.g. for potential ribosomal contamination), and insert size estimation were performed using FastQC, Picard-Tools, Samtools and rseqc. Reads were mapped onto the mm10 mouse genome assembly using STARv2.4.0 (Dobin et al. 2013). The procedures for the gene expression regulation study have been described elsewhere (Noli et al. 2015). Briefly, for each gene present in the Mouse FAST DB v2018_1 annotation, we counted the reads aligning on constitutive regions (which are not prone to alternative splicing). Based on these counts, the level of differential gene expression was normalized using DESeq2 in R (v.3.2.5). Genes were considered to be expressed when their RPKM value was greater than 99% of the value for the background (intergenic region). Only genes annotated in Ensembl database and expressed in at least one of the two experimental conditions were analyzed further. Expression was considered to have changed significantly when the log2 fold change was ³ 1 or ≤ -1 and padj was ≤ 0.05.

Pathway/Gene Ontology (GO) analysis

The GO analysis was performed using the DAVID functional annotation tool (version 6.8) (Huang da et al. 2009; Huang et al. 2007). GO terms and pathways were considered to be enriched if the following conditions were met: fold enrichment ≥ 2.0, uncorrected p-value ≤ 0.05, and minimum number of regulated genes in pathway/term ≥ 2.0. The analysis was performed three times: on all regulated genes, on upregulated genes only, and on downregulated genes only. The three sets of results were emerged to provide a single list. The transcription factor analysis was performed using mouse and human orthologs and the DAVID functional annotation Tool (version 6.8) (Huang da et al. 2009; Huang et al. 2007). The results were visualized using REViGO web tool (Supek et al. 2011).

Single-cell RNA-seq analysis

Raw reads from GEO datasets GSE99058 and GSE98816 were downloaded (He et al. 2016; Vanlandewijck et al. 2018). Seurat 3.1.1 was used to normalize unique molecular identifiers (Butler et al. 2018), using a global-scaling method with a scale factor of 10000 and log-transformation of the data. This was followed by a linear transformation scaling step, so as to avoid highly expressed genes with an excessively high weight in the downstream analysis. With the exception of PCs, cell types were grouped by their level of identity: fibroblasts (fibroblast-like type 1 and 2); ECs (types 1, 2 and 3 ECs, arterial ECs, venous ECs, and capillary ECs), and VSMCs (arteriolar SMCs, arterial SMCs, and venous SMCs). A transcript was considered to be specific or preferentially expressed in a given cell type when it was detected in more than 60% of the corresponding single cells and in a small percentage of cells of other types (Table S3) and had a higher expression level than in other cells (according to a Wilcoxon rank sum test, and with logFC > 1.5).

Quantitative RT-PCR

RNA was extracted using the RNeasy Mini Kit (Qiagen). cDNA was then generated from 100 ng of RNA using the Superscript III Reverse Transcriptase Kit. Differential levels of cDNA expression were measured

using droplet digital PCR (ddPCR)). Briefly, cDNA and primers were distributed into approximately 10000 to 20000 droplets. The nucleic acids were then PCR-amplified in a thermal cycler and read (as the number of positive and negative droplets) on a QX200 ddPCR system (Biorad, Hercules, CA, USA)). The ratio for each tested gene was normalized against the total number of positive droplets for *Gapdh* mRNA. The primer sequences are given in the key resource table. Three to five independent samples were analyzed in each experiment.

High-resolution fluorescent *in situ* hybridization

Fluorescent *in situ* hybridization (FISH) was performed on floating PBS/paraformaldehyde (PFA) 4% fixed brain sections or purified MVs immobilized on a glass slide coated with Cell-Tak (Corning) and fixed for 10 min in PBS/PFA 4%, according to the v2 Multiplex RNAscope technique (Advanced Cell Diagnostics, Inc., Newark, CA, USA) described previously (Oudart et al. 2020). Brain sections and MVs were treated with protease at room temperature. After the FISH, MVs were stained with isolectin B4 (1/100) in PBS/ normal goat serum (NGS) 5%/Triton 0.5% overnight at 4°C. Nuclei were stained with Hoechst reagent (1/2000). The brain sections and purified MVs were imaged using a Spinning Disk CSU-W1 microscope and Metamorph Premier 7.8 software.

FISH quantification

The mRNA density in vessels was analyzed using a newly developed “Vessel_Scope” ImageJ plugin (Rueden et al. 2017). In a calibration step, the intensity of a single mRNA dot was estimated in each experimental condition. Isolated dots were detected using the cell counter ImageJ plugin and segmented using the mcib3D library (Ollion et al. 2013). The background intensity was calculated for regions of interest drawn near each dot:

$$meandotInt.\,bg = \sum_{dotZmin}^{dotZmax} \frac{roiInteg.\,Intensity}{roiarea}$$

where dotZmin and dotZmax correspond to the dot’s lower and upper z positions, respectively.

The background-corrected “single mRNA” intensity was then determined as:

$$\text{corrected "single mRNA" intensity} = \frac{\sum_{1}^{ndots}(\text{dotInteg.Int. - meandotInt.bg * dotVol})}{ndots}$$

Each 3D Z-stack image was then analyzed. MVs were segmented using 3D median filter and Li threshold. RNAScope dots were segmented using difference of Gaussian filter and Triangle threshold. Segmented objects were detected using the mcib3D library (Ollion et al. 2013). For each MV, the number of single mRNAs was defined as the total intensity of dots in the MV divided by the corrected “single mRNA” intensity. The mRNA density of each MV was calculated as the number of single mRNAs divided by the MV’s volume. The MV diameters were measured manually using the straight line tool in ImageJ.

Western blots

MV pellets were sonicated three times for 10 s at 20 Hz (Vibra cell VCX130) in 2% SDS and heated at 56°C in Laemmli loading buffer (Biorad). The protein content was measured using the Pierce 660 nm protein assay kit (Thermo Scientific, Waltham, MA, USA). 10 µg of proteins were separated by denaturing electrophoresis on a 4–15% Criterion™ TGX™ Precast Midi Protein Gel (Biorad) and then electrotransferred to nitrocellulose membranes using the Trans-blot Turbo Transfer System (Biorad). Membranes were hybridized, as described previously (Ezan et al. 2012). The antibodies used in the present study are listed in the key resource table. Horseradish peroxidase activity was visualized by enhanced chemiluminescence in a Western Lightning Plus system (Perkin Elmer, Waltham, MA, USA). Chemiluminescent imaging was performed on a *FUSION FX* system (Vilber, South Korea). The level of chemiluminescence for each antibody was normalized against the histone 3 staining on the membrane.

Clearing and immunohistochemical analysis of murine tissue samples

Mice were killed with pentobarbital (600 mg/kg, i.p.). Brains were removed and post-fixed in 4% PFA for 24 h at 4°C and then assessed using the “immunolabeling-enabled three-dimensional imaging of solvent-cleared organs” technique (Renier et al. 2014). The samples were first dehydrated with increasingly concentrated aqueous Methanol (MetOH) solutions (MetOH: 20%, 40%, 60%, 80%, and twice 100%, for 1 h each) at RT and then incubated in 66% dichloromethane (DCM, Sigma Aldrich)/33% MetOH overnight. After 2 washes in 100% MetOH, brains were incubated in 5% H_2O_2/MetOH overnight at RT, rehydrated with increasingly dilute aqueous MetOH solutions (80%, 60%, 40%, and 20%; 1h each). Before immunostaining, brains were permeabilized first for 2 x 1h at RT in 0.2% Triton X-100/PBS, for 24 h at 37°C in 0.16% Triton X-100/2.3% glycine/20% DMSO/PBS, and then for 2 days at 37°C in 0.16% Triton X-100/6% donkey serum/10% DMSO/PBS. Brains were incubated for 3 days at 37°C with primary antibody diluted in a 0.2 Tween/1% heparin/3% donkey serum/5% DMSO/PBS solution, washed 5 times during 24h at 37°C in 0.2% Tween20/1% heparin/PBS solution, incubated for 3 days at 37°C with secondary antibody diluted in a 0.2 Tween/1% heparin/3% donkey serum/PBS solution, and another washed five times. The brain samples were then dehydrated again with a MetOH/H_2O series (20%, 40%, 60%, 80% and 100% for 1h each, and then 100% overnight) at RT. On the following day, brains were incubated for 3h in 66% DCM/33% MetOH and then twice for 15 min at RT in 100% DCM and lastly cleared overnight in dibenzyl ether.

The cleared tissue was imaged using a light sheet microscope and Inspector pro software (Lavision Biotec GmbH, Bielefeld, Germany). 3D reconstructions were visualized with Imaris software (Bitplane). The length and number of branch points of SMA-immunolabeled brain microvessels were quantified using the “Surface” and “Filament” tools in Imaris software (Oxford instruments, Oxford). Three brains were analyzed per developmental stage.

Immunohistochemical analysis of human tissue samples

The specimens described here are part of the “Hôpitaux Universitaires de l’Est Parisien – Neuropathologie du développement” brain collection (biobank identification number: BB-0033-00082). Informed consent was obtained for brain autopsy and histological examination. Fetal brains were obtained from spontaneous or medical abortions. The fetuses did not display any significant brain disorders or diseases. Analyzed samples: prenatal (15 week of gestation (wg); 21 wg; 28 wg; 30 wg; 39 wg); Postnatal (3 weeks; 1 month; 2 months; 3 months; 8 months; 1 year; 3 years; 4 years (n=2); 10 years; 11 years; 12 years; 13 years (n=2); 16 years; 17 years). One slice per sample was analyzed.

The same technical procedures were applied to all brain samples: after removal, brains were fixed with formalin for 5–12 weeks. A macroscopic analysis enabled the samples to be selected and processed (paraffin embedding, preparation of 7-micron slices, and staining with hematein reagent) for histological analysis. Coronal slices (including the temporal telencephalic parenchyma and the hippocampus) were deparaffinized and unmasked in citrate buffer (pH 6.0). Expression of MYH11 and SMA was detected using the Bond Polymer Refine Detection kit (Leica) and processed on automated immunostaining systems (the Bond RX Leica for MYH11, and the LEICA BOND III for SMA). Pictures were acquired using a slide scanner (Lamina, Perkin Elmer).

Stained samples were analyzed using the QuPath software (Bankhead et al. 2017). For each sample, a QuPath “pixel classifier” was trained to discriminate between DAB-positive spots and the background. This “classifier” consisted in an artificial neural network based on four features: a Gaussian filter to select for the intensity, and three structure tensor eigenvalues to favor thin elongated objects. To train the classifier, we defined manually annotated spots and background area on one image per developmental stage. When the results were visually satisfactory, the trained pixel classifier was used to detect positive spots in manually defined regions of interest.

VSMC contractility *ex vivo*

Mice were rapidly decapitated, and the brains were quickly removed and placed in cold (~4°C) artificial cerebrospinal fluid (aCSF) solution containing 119 mM NaCl, 2.5 mM KCl, 2.5 mM $CaCl_2$, 26.2 mM $NaHCO_3$, 1 mM NaH_2PO_4, 1.3 mM $MgSO_4$, 11 mM D-glucose (pH = 7.35). Brains were constantly oxygenated with 95% O_2 –5% CO_2. Brain cortex slices (400 µm thick) were cut with a vibratome (VT2000S, Leica) and transferred to a constantly oxygenated (95% O_2–5% CO_2) holding chamber containing aCSF. Subsequently, individual slices were placed in a submerged recording chamber maintained at RT under an upright microscope (Zeiss) equipped with a CCD camera (Qimaging) and perfused at 2 mL/min with oxygenated aCSF. MVs at the junction between layers I and II of the somatosensory cortex and with a well-defined luminal diameter (10–15 µm) were selected. Only one MV per slice was analyzed. An image was acquired every 30 s. Each recording started with the establishment of a control baseline for 5 min. MVs with an unstable baseline (i.e. a change in diameter of more than 5%) were discarded from analysis. Vasoconstriction was induced by the application of the thromboxane A_2 receptor agonist U46619 (9,11-dideoxy-11a,9a- epoxymethanoprostaglandin F2α, 50 nM, Sigma) for 2 min. The signal was recorded until it had returned to the baseline.

Any drift in the images during the recording time was corrected either online (for z-drift) or off-line (for the x and y drift), using Image Pro Plus 7.0. To minimize the differences between two consecutive frames, images were manually repositioned using the subtraction tool in Image Pro Plus. Vasoconstriction was measured using a custom routine running in IgorPro (Wavemetrics).

Magnetic resonance imaging of the CBF

MRI was performed on a 7T Pharmascan MRI system (Bruker®, Germany) equipped with volume transmit and surface receive coils. To prevent motion on acquisition, the animals were anesthetized with isoflurane 2-3% in oxygen. The respiratory rate was regulated at 70-100 breaths per minute and temperature was maintained with a warming device. Total acquisition time did not exceed 20 minutes.

A fast T2 anatomical sequence was acquired before the arterial spin labeling (ASL) sequence to allow precise targeting of the slice of interest. Common anatomical features allowed the targeting of the wanted slice (bregma +1 mm) across our groups. The natively implemented ASL sequence on our Bruker MRI scanner was used with a 0.156 x 0.156 mm planar resolution in a single, 1 mm thick slice (matrix size: 128 x 128). Native ASL-calculating macros from Bruker where used for CBF estimations. CBF maps were computed from built-in Bruker macro. A 1 voxel (0.156 x 0.156 mm) gaussian filter was applied on the resulting map to smooth the voxel-wise calculations. CBF values were measured in right and left cortex and meaned for each subject before analysis. Measures on CBF maps were realized with FiJi (Schindelin et al. 2012).

Resources table

Reagent or resource	Source	Reference
Antibodies		
SMA (WB : 1/1000, IF : 1/250)	Sigma	C6198
MYH11 (IF / human slices: 1/50)	Sigma	HPA015310-100UL
Myh11 (Western Blot 1/1000)	Abcam	ab53219
Pecam-1 (IF: 1/300)	R&d systems	AF3628
Histone 3 (Western Blot: 1/2000)	Ozyme	14269S
anti-goat, alexa 647 (IF : 1/2000)	Thermo fisher	
anti-rabbit, HRP (WB : 1/2500)	Cohesion	CSA2115
anti-mouse, HRP (WB : 1/2500)	Cohesion	CSA2108
Alexa-conjugated Isolectin (*griffonia simplicifolia*)	Thermo fisher	I32450
FISH Probes		
Myh11	ACD/Biotechne	316101
qPCR Primers		
Tagln Forward CCCAGACACCGAAGCTACTC Reverse TCGATCCCTCAGGATACAGG	Sigma	
Acta2 Forward GTCCCAGACATCAGGGAGTAA Reverse TCGGATACTTCAGCGTCAGGA	Sigma	
Myh11 Forward AACGCCCTCAAGAGCAAACTCAGA Reverse TCCCGAGCGTCCATTTCTTCTTCA	Sigma	
Atp1b1 Forward GCTGCTAACCATCAGTGAACT Reverse GGGGTCATTAGGACGGAAGGA	Sigma	
Gapdh Forward AGGTCGGTGTGAACGGATTTG Reverse TGTAGACCATGTAGTTGAGGTCA	Sigma	

Tbxar2	Sigma	
Forward CCTTGTTCTCACCGACTTCC		
Reverse GCTGAACCATCATCTCCACC		
qPCR probes		
Kcnj8	Thermofisher	Mm00438070_m1
Abcc9	Thermofisher	Mm00447761_m1
Pecam1	Thermofisher	Mm00487656_m1
Gapdh	Thermofisher	Mm00501337_m1
Software and Algorithms		
ImageJ	https://imagej.nih.gov/ij/	
QuPath	https://qupath.github.io/	
Deposited Data		
Raw data and analysis	This paper	GEO: GSE173844

Results

MVs follow a transcriptional maturation program between P5 and P15

Several studies in rodents have suggested that the brain's microvascular system architecture reorganizes after birth (Coelho-Santos et al. 2021; Coelho-Santos and Shih 2020). To characterize the molecular bases of these changes, we compared the transcriptome of brain mechanically-purified MVs (Boulay et al. 2015) on P5 and P15, two stages defining an important developmental window for the cerebrovascular system (Coelho-Santos et al. 2021; Coelho-Santos and Shih 2020) (**Fig. 1A**). We previously showed that purified MVs are composed by ECs, VSMC, PCs, FBs as well as perivascular astrocyte endfeet and neuronal fibers (Boulay et al. 2015). We limited our transcriptomic study to parenchymal MVs excluding large meningeal arteries and veins (see Materials and methods) and focusing on the dorsal part of the cortex since vascular properties and developmental programs differ from one region of the brain to another. Prior to this analysis, we assessed by qPCR the expression level of known endothelial and pericyte specific transcripts and compared the pericyte/endothelial ratio in mechanically purified cortical MVs and whole cortex at P5 and P15 (**Fig. 1B**). They were identical at both stages indicating that mechanical purification preserved the cellular composition of MVs and is a powerful tool for the molecular characterization of brain vascular cells (**Fig. 1B**). mRNAs extracted from cortical MVs were sequenced, and 11286 transcripts with more than 50 reads in at least one stage were identified (**Fig. 1C; Table S1**). 10355 of the transcripts (92 %) were equally expressed at both time points ($-1 < \log2 \text{ fold-change (FC)} < 1$ or adjusted p-value (padj) > 0.05), and only 931 (8 %) differed significantly between P5 and P15 ($\log2FC \leq -1$ or $\log2FC \geq 1$ and $padj \leq 0.05$). 484 of these 931 (52 %) transcripts

were upregulated on P15 (log2FC ³ 1 and padj ≤ 0.05), and 447 (48 %) were downregulated (log2FC ≤ -1 and padj ≤ 0.05) (**Fig. 1C**). These results indicated that transcription in vascular cells is mostly stable but differs significantly in some respects between P5 and P15. To further characterize these differences, we performed a gene ontology (GO) analysis of our RNA sequencing (RNAseq) data (**Fig. 1D, E; Table S2**). Regarding biological processes, pathways related to mitosis (DNA replication, cell division, and cell cycle) were downregulated on P15, while pathways related to ECM composition, cell junctions and ion transport were upregulated **(Fig. 1D)**. Analysis of the cellular components highlighted lower expression on P15 of pathways related to the chromosomes' centromeric regions and higher expression of pathways related to the membrane, ECM, cell junction, cell surface, and cytoskeleton **(Fig. 1E)**.

Hence, cortical MVs are mostly stable but follow a transcriptional maturation program between P5 and P15.

Characterization of postnatal transcriptional maturation in brain microvessel cells

We next sought to characterize the maturation of each vascular cell type of MVs. By taking advantage of recently published single cell RNASeq datasets for adult brain vascular cells, we started by identifying the genes preferentially or specifically expressed in ECs, PCs, VSMCs and FBs (He et al. 2016; Vanlandewijck et al. 2018) and we determined their expression level in MVs on P5 and P15 (**Fig. 2A**). A transcript was considered to be specific or preferentially expressed in a cell type when it was (i) detected in more than 60% of the single cells of that type and in a small percentage of other cells and (ii) expressed at a higher level than in other cells (LogFC ³ 1.5). This approach led to the identification of 73 EC-, 14 PC-, 38 FB- and 21 VSMC- transcripts (**Table S3**). We then analyzed the FC for each transcript in MVs between P5 and P15: 11, 12 and 10 transcripts were (log2FC ³ 1 and padj ≤ 0.05) upregulated on P15 in ECs, FBs and VSMCs, respectively, and 1 and 1 transcripts were downregulated (log2FC ≤ -1 and padj ≤ 0.05) on P15 in FBs and VSMCs, respectively (**Fig. 2B,C**).

We next focused on VSMC's molecular maturation between P5 and P15.In MVs,VSMCs form a continuum that ranges from contractile cells in arterioles to non-contractile cells around veinules (Frosen and Joutel 2018). Interestingly, all VSMC-specific or -preferentially expressed transcripts upregulated on P15 encoded proteins contributing to contractility, such as *Acta2* (coding for SMA), *Tpm2* (tropomyosin2), *Myh11* (myosin heavy chain 11) and *Tagln* (SM22/transgelin) (**Fig. 2C**). RNAseq results were validated on a selection of genes using qPCRs on MVs purified from whole brain (**Fig. 3A).** As a control, we included in this analysis *Atp1b1*, a VSMC-specific transcript whose expression was unchanged between P5 and P15 (**Table S3**). We then performed a fluorescent *in situ* hybridization (FISH) analysis of *Myh11* (encoding myosin heavy chain 11) on cortical slices **(Fig. 3B**). On P5, few *Myh11* FISH dots were found in the vessels or the parenchyma. In contrast, large parenchymal vessels gave an intense signal on P15 **(Fig. 3B**). To quantify these differences, we next performed FISH on whole-brain purified MVs **(Fig. 3C)**. On P5, *Myh11* FISH dots were detected in most MVs at a moderate density (10-100 x 10^{-3} dots.µm^{-3}) (**Fig. 3D**). On P15, the proportion of unlabeled (0-10 x 10^{-3}dots.µm^{-3}) small-diameter vessels (mean: 5.9 µm ± 3.0) was higher, as was the proportion of densely labeled (>100 x 10^{-3} dots.µm^{-3}) larger-diameter (mean: 13.5

μm ± 5.6) vessels (**Fig. 3C, D; Table S4**). These data highlighted a change in *Myh11* expression from low and diffuse on P5 to high and large MV-specific on P15.

Considering our data as a whole, we identified a set of specific or preferentially-expressed transcripts for each brain vascular cell type and characterized their expression within MVs between P5 and P15. These findings suggest that these brain vascular cells undergo a transcriptional maturation between P5 and P15 specifically regarding VSMC contractility.

VSMCs acquire contractile properties during postnatal development in mice

Our data indicated that the transcription of VSMC-specific genes encoding contractile proteins was upregulated between P5 and P15. To further study this progression, we used Western blotting to analyze the protein levels of SMA and Myh11 in protein extracts from MVs purified from whole brain on P5, P15, P30 and P60. Levels of both proteins rose progressively (**Fig. 4A**). To further characterize the postnatal maturation of VSMCs, we next used an immunofluorescence assay to analyze the SMA-positive cortical vascular network on cleared brain samples from P5, P15 and P60 (**Fig. 4B, C**). The endothelial network was counterstained with an anti-Pecam-1 antibody (**Fig. 5C**). In the parenchyma, we observed that the SMA-positive vascular network became progressively denser. Interestingly, the number of SMA-positive primary branches (penetrating arterioles) did not change significantly over time (**Fig. 4B-D**). However, the total number of SMA-positive branches and ramifications rose progressively (**Fig. 4B-D)**.

To address the functional consequences of these changes, we first compared the *ex vivo* myogenic tone of VSMCs on brain slices sampled on P5, P15 and P60. Of note the absence of perfusion and intraluminal pressure in brain slices result in vessels being maximally dilated (Iadecola and Nedergaard 2007). Thus we focused on VSMC contractility and recorded the change in lumen diameter of cortical arterioles upon exposure for 2 min to a thromboxane A_2 receptor agonist U46619 (9,11-dideoxy-11a,9a-epoxymethanoprostaglandin F2α), which is known to induce reversible vasoconstriction (Perrenoud et al. 2012) (**Fig. 5A-C**). It should be noted that according to our RNAseq data, the level of transcription of *Tbxa2r* (encoding the thromboxane A_2 receptor) did not change between P5 and P15 (log2FC = -0.3, padj = 0.5) (**Table S1**). This finding was confirmed by qPCR on MVs purified from whole brain (**Fig. 5D**). The amplitude of vasoconstriction was assessed as the percentage reduction in vessel diameter upon application of U46619. The slope indicated the velocity of this vasoconstriction. On P5, application of U46619 had a small effect on vessel diameter. In contrast, the amplitude of vasoconstriction was significantly higher on P15 (**Fig. 5A-C**) and even higher again on P60 - indicating that VSMC contractility continues to progress after P15. Thus, in the mouse, vascular contractility rose progressively after birth. Since VSMC contractility promotes the CBF (Nippert et al. 2018), we next measured the cortical CBF on P5 and P15 by arterial spin labeling (ASL) magnetic resonance imaging (MRI) **(Fig. 5E, F)** (Detre et al. 2012). On P5,CBF was significantly lower than P15 and P30, while it did not significantly differ between P15 and P30 mice (**Fig. 5E, F)**. Interestingly, the ratio between the dorsal and lateral cortex was higher at P30 compared to P15 indicating that dorsal cortex CBF continues its maturation after P15 (**Fig. 5E, F**).

Overall, these results demonstrate that the VSMC network expands and complexifies after birth and that VSMCs progressively acquire postnatally their molecular and functional contractile properties contributing to the maturation of the CBF.

The VSMC contractile network matures postnatally in the human cortex

We finally looked at whether the vascular network in humans also matured after birth by measuring MYH11 and SMA expression on human cortical slices from 15 wg to 17 years of age using an immunohistochemical assay (**Fig. 6**). In prenatal samples (from 15 to 39 wg), a MYH11 signal was detected in the meninges but not in the parenchyma (**Fig. 6Ai**). In contrast, penetrating arteries were intensely labeled after birth (**Fig. 6Aii**). After 2 years of age, a large number of MYH11-immunolabeled vessels were observed throughout the parenchyma (**Fig. 6Aiii and iv**). Hence, we quantified a progressive increase in MYH11-positive surface area and the number of MYH11-positive vessels from birth to the age of 2 to 5 years (**Fig. 6B**). SMA was already detected in few penetrating arterioles at prenatal stages (**Fig. 7Ci**) but as MYH11, a progressive increase of SMA-positive surface area and the number of SMA-positive vessels was observed from birth to the age of 2 to 5 years (**Fig. 6Cii and iii, D**).

In conclusion, these results testify to expansion and complexification of the arteriolar VSMC cortical network after birth in the human.

Discussion

The development of the brain's microvascular system during embryogenesis has been well described. In contrast, data on the microvascular system's molecular and functional postnatal maturation are scarce. Here, we demonstrated that vascular cells in the mouse and the human follow postnatal transcriptional programs. In particular we highlighted the postnatal acquisition of contractility by arteriolar VSMCs both in mice and human.

Our analysis of the postnatal maturation of brain vascular cells was firstly based on the transcriptional analysis of parenchymal MVs mechanically purified from the mouse cortex on P5 and P15. This technique has several advantages. Firstly, the vascular cells were not exposed to enzyme treatments that might induce transcriptomic changes. Secondly, this MV preparation enabled us to probe the contribution of all the component cell types while maintaining the *in vivo* ratio between the latter. Our comparison of P5 and P15 MVs revealed that the transcriptome was stable overall: changes were observed for only 8% of the genes. Nevertheless, our GO analysis highlighted the upregulation of pathways specifically related to ECM composition, cell junctions and ion transport and thus evidence the functional maturation of MVs between P5 and P15. In contrast, we observed the downregulation of pathways related to DNA replication, cell division and the cell cycle - suggesting that the putative angiogenic program involved in the postnatal densification of the capillary network was less active on P15.

We next focused on transcripts that were preferentially or specifically expressed in each vascular cell type. We identified these transcripts by checking brain vessel single-cell RNAseq databases (He et al.

2016; Vanlandewijck et al. 2018). Our analysis therefore focused on the transcriptional signature of each vascular cell type, rather than overlaps in molecular repertoires between cell types. Of note, the single-cell RNAseq database used as a reference in our stuy has been generated from mice aged 10–19 weeks (adult stage) and we assumed here that the cellular profile of preselected transcripts is stable during development, which might not be the case for all genes. Several transcripts encoding ECM components were specifically expressed by FBs, confirming that these cells actively contribute to the BL (Manberg et al. 2021) and (possibly) its postnatal development because some genes (*Ctgf, Serping1, Lum, Col6a1, Col5a1* and *Lama1*) were more strongly expressed on P15 than on P5. The recruitment of perivascular FBs and their differentiation has not previously been fully described. The literature data suggest that perivascular FBs are recruited from the meninges after birth (Kelly et al. 2016). Here, we found that half of the FB transcripts were upregulated between P5 and P15; hence, postnatal molecular maturation might also cover the FBs. Our list of PC-preferentially expressed transcripts was consistent with previous transcriptomic analyses (Chasseigneaux et al. 2018; Bondjers et al. 2006); in particular, we identified *Kcnj8* (encoding the ATP-sensitive inward rectifier potassium channel Kir6.1) and *Abcc9* (encoding the ABC transporter 9) involved in ion transport and intercellular signaling (Nelson et al. 2015). Interestingly, expression of all the PC-preferentially expressed transcripts did not differ significantly when comparing P5 and P15; this suggests that PC differentiation and maturation are already complete on P5. Our P5-P15 comparison of MVs showed that some EC-specific or -preferentially expressed transcripts were upregulated, thus indicating that ECs continued to mature after birth. The expression levels of transcripts of TJ proteins or TJ-associated proteins were similar on P5 and P15 cortical MVs. These results are in line with previous reports in which the barrier function was fully established during embryogenesis (by around E15) in the mouse (Daneman et al. 2010). In contrast, expression of some ABC and SLC transport proteins which control molecular access to the brain parenchyma such as P-gP or Oatp1a4 showed levels increased from P15 to P30 in mouse MVs indicating that the brain accessibility to drug follows a postnatal maturation in the mouse. Interestingly, a higher efflux of Rhomamine 123 (a substrate of P-gP) in the rat brain between P4 and P14 (Koehn et al. 2021) and a P-gP increase in humans between 33–43 wg and adulthood (Daood et al. 2008) have been recently documented. Thus, our transcriptional data corroborate previous observation that endothelial efflux properties follows the same developmental process among species.

The vast majority of VSMC-preferentially expressed or -specific transcripts identified in our study were related to muscle differentiation and contractility. Apart from well-known VSMCs transcripts (such as *Acta2*, *Myh11*, *desmin* and *Tgln*), our analysis highlighted the expression of markers like *NR4a1* (coding for nuclear receptor subfamily 4, group A, member 1, involved in SMC proliferation) (Yu et al. 2015), *Pdlim3* (coding for actinin-associated LIM protein), involved in myocyte stability (Zheng et al. 2010), *Mustn1* (regulating myoblast differentiation) (Hadjiargyrou 2018), and *Pln* (coding for phospholamban), which regulates the sarcoplasmic reticulum Ca^{2+}ATPase (SERCA) activity and muscle contractility (Kranias and Hajjar 2012). Surprisingly, about half of the genes were strongly upregulated on P15; this indicates that arteriolar VSMC contractility continued to differentiate between P5 and P15. It is noteworthy that some of these transcripts were expressed (albeit at a much lower level) by PCs.

Nevertheless, our FISH analysis showed that the strongest expression of *Myh11* was limited to the largest MVs, excluding the PCs.

We revealed an increased expression of contractile proteins in arteriolar VSMCs from P5 in the mouse. Parenchymal MYH11 immunoreactivity appearance in the first two years after birth in the human cortex indicated that the same molecular maturation also occurs in humans. Furthermore, we observed a progressive increase in the number of SMA-positive vessels in the mouse (from P5 to P60) and SMA and MYH11-positive vessels in humans (up until the age of two), which shows that the arteriolar network continues its densification postnatally. Our *ex vivo* and *in vivo* observations of the progressive acquisition of cortical arteriole contractility and the marked CBF increase between P5 and P15 indicated that arteriolar VSMCs molecular maturation results in a postnatal phenotypic contractile switch contributing to the brain perfusion. Taken as a whole, our results in the mouse and the human strongly suggest that the myogenic tone of parenchymal arterioles, which determines vascular tone and brain perfusion, is acquired progressively after birth.

It is thought that during embryogenesis, VSMCs are recruited to newly formed vessels in two ways: (i) the *de novo* formation of VSMCs via the induction of undifferentiated perivascular mesenchymal cells, and (ii) the migration of VSMCs from a preexisting pool (Hellstrom et al. 1999). The same mechanisms might operate during the brain arteriolar VSMC network's postnatal expansion. During embryogenesis, VSMC differentiation is regulated by several signaling pathways (including VEGFA, Notch, EphrinB2/B4, PDGFß and TGFß pathways) between ECs and mural cells (Owens et al. 2004). In the future, it would be interesting to address these pathways' role during the postnatal period.

Vessel contractility is crucial to the neurovascular coupling, i.e the capacity of the vascular system to locally adapt blood flow to neuronal activity. Recent studies suggested that the neurovascular coupling in neonates and preterm born infants differs compared to adults (Anderson et al. 2001; Kusaka et al. 2004), although adult-like cerebral haemodynamic responses were also reported in infants born preterm (Arichi et al. 2010) and 2–4 month-old infants (Taga et al. 2003). In rodents, a progression of the hemodynamic response was described from P7 to the adult (Colonnese et al. 2008; Kozberg et al. 2013; Zehendner et al. 2013) and has been attributed to the immaturity of most of the cellular components involved in the hemodynamic response, i.e. astrocytic and synaptic connectivity, vascular network and myelination are still in development at birth. Our study now indicates that the postnatal acquisition of arteriolar VSMC contractility is likely to be another and probably mandatory element in this maturation process.

From a medical and pharmacological point of view, our results are crucial. Indeed, non-invasive MRI studies of intracranial aneurysms have shown that cortical blood flow was altered in preterm (before 36 wg) compared to term newborns (Chalouhi et al. 2012). The maturation of the brain vasculature's responsiveness is associated with differential responses to vasoactive drugs in preterm, term newborns, and adults. The best vasoactive drugs for the management of neonatal systemic hypotension might not be those used for the same purpose in adults (Toth-Heyn and Cataldi 2012). Lastly, impairments of arteriolar VSMC differentiation and contractility have been linked to several small-vessel diseases, such

as cerebral aneurysm (Chalouhi et al. 2012), arteriovenous malformations, and cerebral cavernous malformations (Uranishi et al. 2001; Frosen and Joutel 2018). In view of our results, impairments in the arteriolar VSMCs' postnatal differentiation might also be involved in these diseases.

In conclusion, our present results revealed that the parenchymal cerebral microvasculature in the mouse and in the human undergoes a profound molecular maturation after birth. This maturation results in particular in the acquisition of VSMC contractility which governs cerebral perfusion and neurovascular coupling; hence, this maturation is a crucial step in the acquisition of brain functions and might guide treatment approaches in pediatric medicine.

Declarations

Acknowledgments

This work was funded by grants from the *Association Européenne contre les Leucodystrophies* (ELA) (ELA2012-014C2B), the *Fondation pour la Recherche Médicale* (FRM) (AJE20171039094) and the *Fondation Maladies Rares* (20170603). A. Gilbert's PhD fellowship was funded by the FRM (PLP20170939025p60) and ELA (ELA2012-014C2B). L. Slaoui's fellowship PhD was funded by the Ecole Normale Supérieure. A.-C. Boulay's work was funded by the FRM (AJE20171039094) and the *Foundation pour la recherche sur la sclérose en plaques* (ARSEP). Despite our efforts, our work has not received any support from the French National Agency for Research (ANR).

Author contributions

Conceptualization, M.C-S. and A-C.B.; Methodology, M.C-S., A-C.B., S.C., P.M., G.L., A.G., N.R., D.V., A.R.; Investigation, L.S., A.G., M.B.L, L.F., A.R., A.C., Q.G., M.F., K.D., L.J., S.A., A-C.B., M. C-S; Writing – Original Draft, M.C-S.; Funding Acquisition, M.C-S.; Supervision, M.C-S.and A-C.B.

The authors declare no competing financial interests

This article contains 4 supplementary Tables

Data availability

The RNA-seq gene expression data and raw fastq files are available on the GEO repository (www.ncbi.nlm.nih.gov/geo/) under the accession number GSE173844. All other experimental raw data are given in Table S4.

References

1. Anderson AW, Marois R, Colson ER, Peterson BS, Duncan CC, Ehrenkranz RA, Schneider KC, Gore JC, Ment LR (2001) Neonatal auditory activation detected by functional magnetic resonance imaging. Magn Reson Imaging 19 (1):1–5. doi:10.1016/s0730-725x(00)00231-9

2. Arichi T, Moraux A, Melendez A, Doria V, Groppo M, Merchant N, Combs S, Burdet E, Larkman DJ, Counsell SJ, Beckmann CF, Edwards AD (2010) Somatosensory cortical activation identified by functional MRI in preterm and term infants. Neuroimage 49 (3):2063–2071. doi:10.1016/j.neuroimage.2009.10.038
3. Bankhead P, Loughrey MB, Fernandez JA, Dombrowski Y, McArt DG, Dunne PD, McQuaid S, Gray RT, Murray LJ, Coleman HG, James JA, Salto-Tellez M, Hamilton PW (2017) QuPath: Open source software for digital pathology image analysis. Sci Rep 7 (1):16878. doi:10.1038/s41598-017-17204-5
4. Ben-Zvi A, Liebner S (2021) Developmental regulation of barrier- and non-barrier blood vessels in the CNS. J Intern Med. doi:10.1111/joim.13263
5. Bondjers C, He L, Takemoto M, Norlin J, Asker N, Hellstrom M, Lindahl P, Betsholtz C (2006) Microarray analysis of blood microvessels from PDGF-B and PDGF-Rbeta mutant mice identifies novel markers for brain pericytes. FASEB J 20 (10):1703–1705. doi:fj.05-4944fje [pii]
6. 1096/fj.05-4944fje
7. Boulay AC, Saubamea B, Decleves X, Cohen-Salmon M (2015) Purification of Mouse Brain Vessels. J Vis Exp 105 (105). doi:10.3791/53208
8. Butler A, Hoffman P, Smibert P, Papalexi E, Satija R (2018) Integrating single-cell transcriptomic data across different conditions, technologies, and species. Nat Biotechnol 36 (5):411–420. doi:10.1038/nbt.4096
9. Chalouhi N, Ali MS, Jabbour PM, Tjoumakaris SI, Gonzalez LF, Rosenwasser RH, Koch WJ, Dumont AS (2012) Biology of intracranial aneurysms: role of inflammation. J Cereb Blood Flow Metab 32 (9):1659–1676. doi:10.1038/jcbfm.2012.84
10. Chasseigneaux S, Moraca Y, Cochois-Guegan V, Boulay AC, Gilbert A, Le Crom S, Blugeon C, Firmo C, Cisternino S, Laplanche JL, Curis E, Decleves X, Saubamea B (2018) Isolation and differential transcriptome of vascular smooth muscle cells and mid-capillary pericytes from the rat brain. Sci Rep 8 (1):12272. doi:10.1038/s41598-018-30739-5
11. Coelho-Santos V, Berthiaume AA, Ornelas S, Stuhlmann H, Shih AY (2021) Imaging the construction of capillary networks in the neonatal mouse brain. Proc Natl Acad Sci U S A 118 (26). doi:10.1073/pnas.2100866118
12. Coelho-Santos V, Shih AY (2020) Postnatal development of cerebrovascular structure and the neurogliovascular unit. Wiley Interdiscip Rev Dev Biol 9 (2):e363. doi:10.1002/wdev.363
13. Cohen-Salmon M, Slaoui L, Mazare N, Gilbert A, Oudart M, Alvear-Perez R, Elorza-Vidal X, Chever O, Boulay AC (2021) Astrocytes in the regulation of cerebrovascular functions. Glia 69 (4):817–841. doi:10.1002/glia.23924
14. Colonnese MT, Phillips MA, Constantine-Paton M, Kaila K, Jasanoff A (2008) Development of hemodynamic responses and functional connectivity in rat somatosensory cortex. Nat Neurosci 11 (1):72–79. doi:10.1038/nn2017

15. Daneman R, Zhou L, Kebede AA, Barres BA (2010) Pericytes are required for blood-brain barrier integrity during embryogenesis. Nature 468 (7323):562–566. doi:nature09513 [pii]
16. 1038/nature09513
17. Daood M, Tsai C, Ahdab-Barmada M, Watchko JF (2008) ABC transporter (P-gp/ABCB1, MRP1/ABCC1, BCRP/ABCG2) expression in the developing human CNS. Neuropediatrics 39 (4):211–218. doi:10.1055/s-0028-1103272
18. Detre JA, Rao H, Wang DJ, Chen YF, Wang Z (2012) Applications of arterial spin labeled MRI in the brain. J Magn Reson Imaging 35 (5):1026–1037. doi:10.1002/jmri.23581
19. Dobin A, Davis CA, Schlesinger F, Drenkow J, Zaleski C, Jha S, Batut P, Chaisson M, Gingeras TR (2013) STAR: ultrafast universal RNA-seq aligner. Bioinformatics 29 (1):15–21. doi:10.1093/bioinformatics/bts635
20. Ezan P, Andre P, Cisternino S, Saubamea B, Boulay AC, Doutremer S, Thomas MA, Quenech'du N, Giaume C, Cohen-Salmon M (2012) Deletion of astroglial connexins weakens the blood-brain barrier. J Cereb Blood Flow Metab 32 (8):1457–1467. doi:jcbfm201245 [pii]
21. 1038/jcbfm.2012.45
22. Frosen J, Joutel A (2018) Smooth muscle cells of intracranial vessels: from development to disease. Cardiovasc Res 114 (4):501–512. doi:10.1093/cvr/cvy002
23. Hadjiargyrou M (2018) Mustn1: A Developmentally Regulated Pan-Musculoskeletal Cell Marker and Regulatory Gene. Int J Mol Sci 19 (1). doi:10.3390/ijms19010206
24. Hartmann DA, Underly RG, Grant RI, Watson AN, Lindner V, Shih AY (2015) Pericyte structure and distribution in the cerebral cortex revealed by high-resolution imaging of transgenic mice. Neurophotonics 2 (4):041402. doi:10.1117/1.NPh.2.4.041402
25. SSR [pii]
26. He L, Vanlandewijck M, Raschperger E, Andaloussi Mae M, Jung B, Lebouvier T, Ando K, Hofmann J, Keller A, Betsholtz C (2016) Analysis of the brain mural cell transcriptome. Sci Rep 6:35108. doi:srep35108 [pii]
27. 1038/srep35108
28. Hellstrom M, Kalen M, Lindahl P, Abramsson A, Betsholtz C (1999) Role of PDGF-B and PDGFR-beta in recruitment of vascular smooth muscle cells and pericytes during embryonic blood vessel formation in the mouse. Development 126 (14):3047–3055
29. Huang da W, Sherman BT, Lempicki RA (2009) Systematic and integrative analysis of large gene lists using DAVID bioinformatics resources. Nat Protoc 4 (1):44–57. doi:10.1038/nprot.2008.211
30. Huang DW, Sherman BT, Tan Q, Kir J, Liu D, Bryant D, Guo Y, Stephens R, Baseler MW, Lane HC, Lempicki RA (2007) DAVID Bioinformatics Resources: expanded annotation database and novel algorithms to better extract biology from large gene lists. Nucleic Acids Res 35 (Web Server issue):W169-175. doi:10.1093/nar/gkm415

31. Iadecola C, Nedergaard M (2007) Glial regulation of the cerebral microvasculature. Nat Neurosci 10 (11):1369–1376. doi:10.1038/nn2003
32. Kelly KK, MacPherson AM, Grewal H, Strnad F, Jones JW, Yu J, Pierzchalski K, Kane MA, Herson PS, Siegenthaler JA (2016) Col1a1 + perivascular cells in the brain are a source of retinoic acid following stroke. BMC Neurosci 17 (1):49. doi:10.1186/s12868-016-0284-5
33. Koehn LM, Dziegielewska KM, Habgood MD, Huang Y, Saunders NR (2021) Transfer of rhodamine-123 into the brain and cerebrospinal fluid of fetal, neonatal and adult rats. Fluids Barriers CNS 18 (1):6. doi:10.1186/s12987-021-00241-8
34. Kozberg MG, Chen BR, DeLeo SE, Bouchard MB, Hillman EM (2013) Resolving the transition from negative to positive blood oxygen level-dependent responses in the developing brain. Proc Natl Acad Sci U S A 110 (11):4380–4385. doi:10.1073/pnas.1212785110
35. Kranias EG, Hajjar RJ (2012) Modulation of cardiac contractility by the phospholamban/SERCA2a regulatome. Circ Res 110 (12):1646–1660. doi:10.1161/CIRCRESAHA.111.259754
36. Kusaka T, Kawada K, Okubo K, Nagano K, Namba M, Okada H, Imai T, Isobe K, Itoh S (2004) Noninvasive optical imaging in the visual cortex in young infants. Hum Brain Mapp 22 (2):122–132. doi:10.1002/hbm.20020
37. Manberg A, Skene N, Sanders F, Trusohamn M, Remnestal J, Szczepinska A, Aksoylu IS, Lonnerberg P, Ebarasi L, Wouters S, Lehmann M, Olofsson J, von Gohren Antequera I, Domaniku A, De Schaepdryver M, De Vocht J, Poesen K, Uhlen M, Anink J, Mijnsbergen C, Vergunst-Bosch H, Hubers A, Klappe U, Rodriguez-Vieitez E, Gilthorpe JD, Hedlund E, Harris RA, Aronica E, Van Damme P, Ludolph A, Veldink J, Ingre C, Nilsson P, Lewandowski SA (2021) Altered perivascular fibroblast activity precedes ALS disease onset. Nat Med 27 (4):640–646. doi:10.1038/s41591-021-01295-9
38. Mathiisen TM, Lehre KP, Danbolt NC, Ottersen OP (2010) The perivascular astroglial sheath provides a complete covering of the brain microvessels: an electron microscopic 3D reconstruction. Glia 58 (9):1094–1103. doi:10.1002/glia.20990
39. Nelson PT, Jicha GA, Wang WX, Ighodaro E, Artiushin S, Nichols CG, Fardo DW (2015) ABCC9/SUR2 in the brain: Implications for hippocampal sclerosis of aging and a potential therapeutic target. Ageing Res Rev 24 (Pt B):111–125. doi:10.1016/j.arr.2015.07.007
40. Nippert AR, Biesecker KR, Newman EA (2018) Mechanisms Mediating Functional Hyperemia in the Brain. Neuroscientist 24 (1):73–83. doi:10.1177/1073858417703033
41. Noli L, Capalbo A, Ogilvie C, Khalaf Y, Ilic D (2015) Discordant Growth of Monozygotic Twins Starts at the Blastocyst Stage: A Case Study. Stem Cell Reports 5 (6):946–953. doi:10.1016/j.stemcr.2015.10.006
42. Ollion J, Cochennec J, Loll F, Escude C, Boudier T (2013) TANGO: a generic tool for high-throughput 3D image analysis for studying nuclear organization. Bioinformatics 29 (14):1840–1841. doi:10.1093/bioinformatics/btt276
43. Oudart M, Tortuyaux R, Mailly P, Mazare N, Boulay AC, Cohen-Salmon M (2020) AstroDot - a new method for studying the spatial distribution of mRNA in astrocytes. J Cell Sci 133 (7).

doi:10.1242/jcs.239756

44. Owens GK, Kumar MS, Wamhoff BR (2004) Molecular regulation of vascular smooth muscle cell differentiation in development and disease. Physiol Rev 84 (3):767–801. doi:10.1152/physrev.00041.2003
45. Perrenoud Q, Rossier J, Ferezou I, Geoffroy H, Gallopin T, Vitalis T, Rancillac A (2012) Activation of cortical 5-HT(3) receptor-expressing interneurons induces NO mediated vasodilatations and NPY mediated vasoconstrictions. Front Neural Circuits 6:50. doi:10.3389/fncir.2012.00050
46. Renier N, Wu Z, Simon DJ, Yang J, Ariel P, Tessier-Lavigne M (2014) iDISCO: a simple, rapid method to immunolabel large tissue samples for volume imaging. Cell 159 (4):896–910. doi:10.1016/j.cell.2014.10.010
47. Rueden CT, Schindelin J, Hiner MC, DeZonia BE, Walter AE, Arena ET, Eliceiri KW (2017) ImageJ2: ImageJ for the next generation of scientific image data. BMC Bioinformatics 18 (1):529. doi:10.1186/s12859-017-1934-z
48. Rungta RL, Chaigneau E, Osmanski BF, Charpak S (2018) Vascular Compartmentalization of Functional Hyperemia from the Synapse to the Pia. Neuron 99 (2):362–375 e364. doi:10.1016/j.neuron.2018.06.012
49. Saunders A, Macosko EZ, Wysoker A, Goldman M, Krienen FM, de Rivera H, Bien E, Baum M, Bortolin L, Wang S, Goeva A, Nemesh J, Kamitaki N, Brumbaugh S, Kulp D, McCarroll SA (2018) Molecular Diversity and Specializations among the Cells of the Adult Mouse Brain. Cell 174 (4):1015–1030 e1016. doi:10.1016/j.cell.2018.07.028
50. Schindelin J, Arganda-Carreras I, Frise E, Kaynig V, Longair M, Pietzsch T, Preibisch S, Rueden C, Saalfeld S, Schmid B, Tinevez JY, White DJ, Hartenstein V, Eliceiri K, Tomancak P, Cardona A (2012) Fiji: an open-source platform for biological-image analysis. Nat Methods 9 (7):676–682. doi:10.1038/nmeth.2019
51. Supek F, Bosnjak M, Skunca N, Smuc T (2011) REVIGO summarizes and visualizes long lists of gene ontology terms. PLoS One 6 (7):e21800. doi:10.1371/journal.pone.0021800
52. Taga G, Asakawa K, Maki A, Konishi Y, Koizumi H (2003) Brain imaging in awake infants by near-infrared optical topography. Proc Natl Acad Sci U S A 100 (19):10722–10727. doi:10.1073/pnas.1932552100
53. Toth-Heyn P, Cataldi L (2012) Vasoactive compounds in the neonatal period. Curr Med Chem 19 (27):4633–4639. doi:10.2174/092986712803306330
54. Uranishi R, Baev NI, Kim JH, Awad IA (2001) Vascular smooth muscle cell differentiation in human cerebral vascular malformations. Neurosurgery 49 (3):671–679; discussion 679–680. doi:10.1097/00006123-200109000-00027
55. Vanlandewijck M, He L, Mae MA, Andrae J, Ando K, Del Gaudio F, Nahar K, Lebouvier T, Lavina B, Gouveia L, Sun Y, Raschperger E, Rasanen M, Zarb Y, Mochizuki N, Keller A, Lendahl U, Betsholtz C (2018) A molecular atlas of cell types and zonation in the brain vasculature. Nature 554 (7693):475–480. doi:10.1038/nature25739

56. Yu Y, Cai Z, Cui M, Nie P, Sun Z, Sun S, Chu S, Wang X, Hu L, Yi J, Shen L, He B (2015) The orphan nuclear receptor Nur77 inhibits low shear stress-induced carotid artery remodeling in mice. Int J Mol Med 36 (6):1547–1555. doi:10.3892/ijmm.2015.2375
57. Zehendner CM, Tsohataridis S, Luhmann HJ, Yang JW (2013) Developmental switch in neurovascular coupling in the immature rodent barrel cortex. PLoS One 8 (11):e80749. doi:10.1371/journal.pone.0080749
58. Zheng M, Cheng H, Banerjee I, Chen J (2010) ALP/Enigma PDZ-LIM domain proteins in the heart. J Mol Cell Biol 2 (2):96–102. doi:10.1093/jmcb/mjp038

Figures

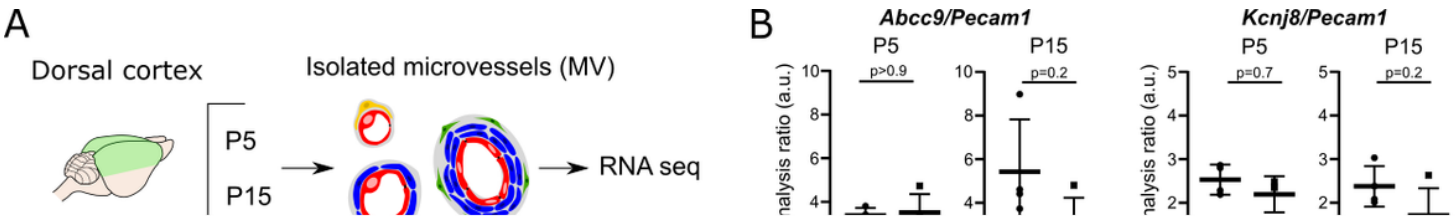

Figure 1

Brain MVs follow a transcriptional maturation program between P5 and P15

A. Flowchart of the transcriptional analysis of MVs extracted from dorsal cortex at P5 and P15. Endothelial cells are represented in red, pericytes in yellow, vascular smooth muscle cells in blue and fibroblasts in green. **B.** Ratio of qPCR quantification for the pericyte-specific transcripts *Abcc9* and *Kncj8* on the endothelial specific transcript *Pecam1* in MVs and cortex at P5 and P15. The plotted data are quoted as the mean ± SD. Two-tailed Mann-Whitney test (n=4 samples per stage; number of mice per MV sample: 3 for P5; 3 for P15; One mouse per dorsal cortex sample). Data are given in **Table S4**. **C.**

Graphical comparison of the RNAseq data for MV transcripts on P5 vs. P15. Transcripts with no changes (in white): -1 < log2FC < 1 or padj > 0.05; transcripts with changes (in black): log2FC ≤ -1 or log2FC ³ 1, padj ≤ 0.05; transcripts upregulated on P15 (in red): log2FC ³ 1, padj ≤ 0.05; transcripts downregulated on P15 (in blue): log2FC ≤ -1, padj ≤ 0.05. n=3 libraries for each stage. **D. E.** A gene ontology (GO) analysis of transcriptional changes in cortical MVs between P5 and P15 for “biological processes” (**D**) and “cellular components” (**E**). A REViGO representation of the results of GO analysis. Data are given in **Table S2**.

Figure 2

Identification of the transcriptional signature of brain vascular cells and characterization of their postnatal expression within MVs

A. Flowchart of the identification of cell specific transcripts from the vascular single cell database (He et al. 2016; Vanlandewijck et al. 2018) and study of their expression in our transcriptional analysis of MVs extracted from dorsal cortex on P5 and P15. Endothelial cells are represented in red, pericytes in yellow, vascular smooth muscle cells in blue and fibroblasts in green**. B.** log2FC for cell-type-specific or -preferentially expressed transcripts in cortical MVs on P5 and P15. Each dot represents a transcript. Red dots correspond to significant changes between P5 and P15 (log2FC ≤ -1 or log2FC ³ 1, padj ≤ 0.05). Black dots correspond to transcripts that did not change between P5 and P15 (-1 < log2FC <1 or padj > 0.05). Lines incate the mean for each category**. C.** RNAseq data for significantly changed cell-type-specific or -preferentially expressed transcripts in cortical MVs between P5 and P15. EC, endothelial cell; PC, pericyte; FB, fibroblast: VSMC, vascular smooth muscle cell. Data are given in **Table S3**.

Figure 3

Validation of transcriptional maturation in arteriolar VSMCs from P5 to P15

A. qPCR results for vascular smooth muscle cell-specific or -preferentially expressed transcripts on P5, P10 and P15 purified MVs from whole brain are shown. Signals were normalized against *Gapdh*. The value on P5 was set to 1 (dotted line). The plotted data are quoted as the mean ± SD. Kruskal-Wallis test (overall, in bold) and one-tailed Mann-Whitney test (comparison of stages) for 3 to 5 samples per stage (mice per sample: 5 for P5; 3 for P15; 2 for P30; 2 for P60). **B-E.** FISH analysis of Myh11 expression on P5 and P15. Confocal microscopy images (FISH detection) of *Myh11* mRNAs (red dots) in the cortex (**B**) or in purified MVs (**C**). Vessels were stained with isolectin B4 (IB4). Nuclei were stained with Hoechst. White

arrowheads indicate FISH dots in vascular smooth muscle cells. **D, E.** Quantification. **D.** MVs were divided into three categories, according to their FISH dot density. The proportion of MVs in each category on P5 and P15 are shown. A chi² test for changes in the distribution across vessel categories (bold) and a one-tailed Mann-Whitney test for changes over time of each category (285 vessels at P5 and 330 vessels at P15 prepared from 3 mice). **E.** MV diameter for each FISH dot density category on P15. Kruskal-Wallis test (overall, in bold) and a one-tailed Mann-Whitney test (comparison of categories) (330 vessels prepared from 3 mice).

Figure 4

Postnatal acquisition of VSMC contractile molecular properties and expansion of the VSMC contractile network

A. Western blot detection and analysis of SMA, Myh11 and histone 3 (H3) in protein extracts from MVs purified from whole brain on P5, P15, P30 and P60. Signals were normalized against H3. The results on P5 were set to 1. Kruskal-Wallis test (overall, in bold) and a one-tailed Mann-Whitney test (comparison of stages). The data are quoted as the mean ± SD (n = 3 or 4 samples per developmental stage; mice per sample: 5 for P5; 4 for P10; 3 for P15; 2 for P60). **B. C.** Representative 3D images of the arterial network in cleared brains and (at higher magnification) in the cortex on P5, P15 and P60, after immunolabeling for SMA (**B, C**) and Pecam-1 (**C**). **D.** Comparative analysis of the SMA-positive vessel length, number of primary or total branches, and ramification in the parenchymal cortex. The data are quoted as the mean ± SD (n = 3 mice per stage). Kruskal-Wallis test (overall, in bold) and a one-tailed Mann-Whitney test (comparison of stages). Data are given in **Table S4**.

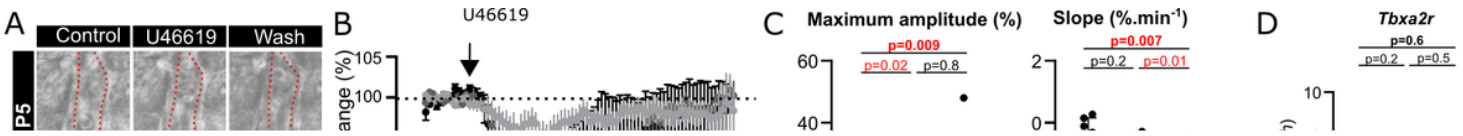

Figure 5

VSMC contractility and CBF mature postnatally in the mouse cortex

A-C. *Ex vivo* analysis of arteriolar constriction on slices of somatosensory cortex from mice on P5, P15 and P60. **A. Representative** infrared images of arteriole constriction in response to bath application of U46619 and dilation upon washing, for samples obtained on P5 and P60. The vessel lumen is indicated by a red dotted line. **B.** Time course of the change in vessel lumen size for P5, P15 and P60 samples. 0 min corresponds to the addition of U46619 in the recording chamber medium. The data are quoted as the mean ± SEM. **C.** Analysis of **(B)**. Maximal amplitude and slope of the contraction. The mean value before U466619 application was set as 0. Kruskal-Wallis test (overall, in bold) and a one-tailed Mann-Whitney test (comparison of stages). The data are quoted as the mean ± SD (n = 13 vessels on P5; 9 on P15; 8 at P60; 3 mice per group). **D.** qPCR results for *Tbxa2r* in mRNAs from MVs purified from whole brain on P5, P15 and P60. Signals were normalized against *Gapdh*. The results on P5 were set to 1. Kruskal-Wallis test (overall, in bold) and a one-tailed Mann-Whitney test (comparison of stages). The data are quoted as the mean ± SD. n= 3 to 5 samples per stage (mice per sample: 5 for P5; 3 for P15; 2 for P30; 2 for P60). **E-F.** *In vivo* analysis of the CBF by ASL MRI from mice on P5, P15 and P30. **E.** Representative T2 (up) and ASL (down) MRI images. Boxed areas indicate dorsal and lateral cortical areas. **F.** Analysis of the CBF in the whole cortex (left); dorsal/lateral CBF ratio (right). The data are quoted as the mean ± SD. One-way ANOVA (overall, in bold) and Tukey's multiple comparison test (comparison of stages) (n= 9 or 10 mice per group). Data are given in **Table S4**.

Figure 6

The network of contractile VSMCs matures postnatally in the human cortex

A. B. Immunohistochemistry analysis of MYH11 (**A**) and SMA (**B**) expression in the developing human cortex. Representative images of MYH11 (**A**) or SMA (**B**) -stained brain cortical slices (left) and (at higher magnification) in the parenchyma of the boxed area (right) for samples taken (i) in the prenatal period (15 wg to 39 wg), (ii) between 0 and 2 years of age, (iii) between 2 and 5 years of age and (iv) after 10 years of age. Expression in penetrating arterioles (arrow) and parenchymal arterioles (arrowheads) was revealed by DAB staining. **C. D.** Quantification of the MYH11- (**C**) or SMA- (**D**) stained surface areas and the number of detected objects, quoted as the mean ± SD. Kruskal-Wallis test (overall, in bold) and one-tailed Mann-Whitney test (comparison of stages). Number of samples per developmental age: 5 or 6 for prenatal, 4 for 0-2 years, 4 for 2-5 years and 7 or 8 for >10 years (see details in Materials and Methods). Data are given in **Table S4**.

Supplementary Files

This is a list of supplementary files associated with this preprint. Click to download.

- 20220221TableS1.xlsx
- 20211221TableS2.xlsx
- 20220217TableS3.xlsx
- 20210217TableS4.xlsx